

RESEARCH ARTICLE

Visual, Vestibular, and Somatosensory Interactions for Visuomotor Responses: A Tribute to Jerry Simpson

## Response properties of optic flow neurons in the accessory optic system of hummingbirds versus zebra finches and pigeons

Andrea H. Gaede,<sup>1,2,3\*</sup> Vikram B. Baliga,<sup>2\*</sup> Graham Smyth,<sup>2</sup> Cristian Gutiérrez-Ibáñez,<sup>3</sup>  
Douglas L. Altshuler,<sup>2</sup> and Douglas R. Wylie<sup>3</sup>

<sup>1</sup>Structure and Motion Laboratory, Royal Veterinary College, University of London, Hertfordshire, United Kingdom;

<sup>2</sup>Department of Zoology, University of British Columbia, Vancouver, British Columbia, Canada; and <sup>3</sup>Department of Biological Sciences, University of Alberta, Edmonton, Alberta, Canada

### Abstract

Optokinetic responses function to maintain retinal image stabilization by minimizing optic flow that occurs during self-motion. The hovering ability of hummingbirds is an extreme example of this behavior. Optokinetic responses are mediated by direction-selective neurons with large receptive fields in the accessory optic system (AOS) and pretectum. Recent studies in hummingbirds showed that, compared with other bird species, 1) the pretectal nucleus lentiformis mesencephali (LM) is hypertrophied, 2) LM has a unique distribution of direction preferences, and 3) LM neurons are more tightly tuned to stimulus velocity. In this study, we sought to determine if there are concomitant changes in the nucleus of the basal optic root (nBOR) of the AOS. We recorded the visual response properties of nBOR neurons to large-field-drifting random dot patterns and sine-wave gratings in Anna's hummingbirds and zebra finches and compared these with archival data from pigeons. We found no differences with respect to the distribution of direction preferences: Neurons responsive to upward, downward, and nasal-to-temporal motion were equally represented in all three species, and neurons responsive to temporal-to-nasal motion were rare or absent (<5%). Compared with zebra finches and pigeons, however, hummingbird nBOR neurons were more tightly tuned to stimulus velocity of random dot stimuli. Moreover, in response to drifting gratings, hummingbird nBOR neurons are more tightly tuned in the spatiotemporal domain. These results, in combination with specialization in LM, support a hypothesis that hummingbirds have evolved to be "optic flow specialists" to cope with the optomotor demands of sustained hovering flight.

**NEW & NOTEWORTHY** Hummingbirds have specialized response properties to optic flow in the pretectal nucleus lentiformis mesencephali (LM). The LM works with the nucleus of the basal optic root (nBOR) of the accessory optic system (AOS) to process global visual motion, but whether the neural response specializations observed in the LM extend to the nBOR is unknown. Hummingbird nBOR neurons are more tightly tuned to visual stimulus velocity, and in the spatiotemporal domain, compared with two nonhovering species.

*accessory optic system; basal optic root; optic flow; optokinetic; visual motion*

### INTRODUCTION

In a 1988 issue of the *Journal of Neurophysiology*, four companion papers from John (Jerry) Simpson and colleagues detailed how visual information is conveyed to the cerebellar flocculus. These papers illustrated how 1) visual information is initially processed by direction-selective neurons in the

accessory optic system (AOS) (1), 2) how these signals are integrated initially in the ventral tegmental relay zone (2) and 3) further in the dorsal cap and ventrolateral outgrowth of the inferior olive (3), such that 4) the visual climbing fibers to the flocculus evoke complex spike responses that are organized as a three-axis system matching the orientation of the vestibular canals (4). The visual signal processed in this pathway is

\* A. H. Gaede and V. B. Baliga contributed equally to this work.

Correspondence: D. L. Altshuler (doug@zoology.ubc.ca); D. R. Wylie (dwylie@ualberta.ca).

Submitted 30 September 2021 / Revised 29 November 2021 / Accepted 30 November 2021



“optic flow”; the visual motion across the entire retina due to self-motion (Fig. 1A) (7). Optic flow drives the optokinetic response, which is necessary to maintain retinal image stabilization (8). A stable retinal image allows for optimal visual acuity (9) and velocity discrimination (10).

As outlined in Jerry’s paper in the *Annual Review of Neuroscience* in 1984 (11), although the anatomy of the AOS had been well established by the 1960s, its function was unknown and was a great source of frustration (12). Jerry’s research clearly showed that the AOS processes optic flow signals (13). The demonstration of visual neuron responses to large moving stimuli (e.g., see Ref. 13) was quite unique at the time, as neurons in the geniculostriate (e.g., see Ref. 14) and tectofugal pathways (e.g., see Ref. 15) respond mainly to small stimuli. Moreover, Jerry’s work firmly identified the AOS as a pathway for generating the optokinetic response. Early researchers were vexed that the optokinetic response

was virtually unaffected by large lesions ablating the much more extensive geniculostriate and tectofugal visual pathways (e.g., see Refs. 16 and 17).

Since Jerry’s original work on the AOS in rabbits, optic flow processing has been investigated in several vertebrate species. Although there are at least three nuclei in the mammalian AOS (11, 18), in other vertebrates, including birds, there is a single nucleus called the nucleus of the basal optic root (nBOR; Fig. 1, D–F) (19–21). In addition to the AOS, optic flow is also processed in a pretectal nucleus, the nucleus of the optic tract (NOT) in the mammals (22–24). The homolog in birds and reptiles is the nucleus lentiformis mesencephali (LM; Fig. 1E) (21, 25, 26). Neurons in the AOS and pretectum have large receptive fields (average  $\sim 60^\circ$ ), exhibit direction-selectivity to large moving stimuli rich in visual texture (e.g., random dot patterns), and are tuned to stimulus velocity. Collectively, the AOS and

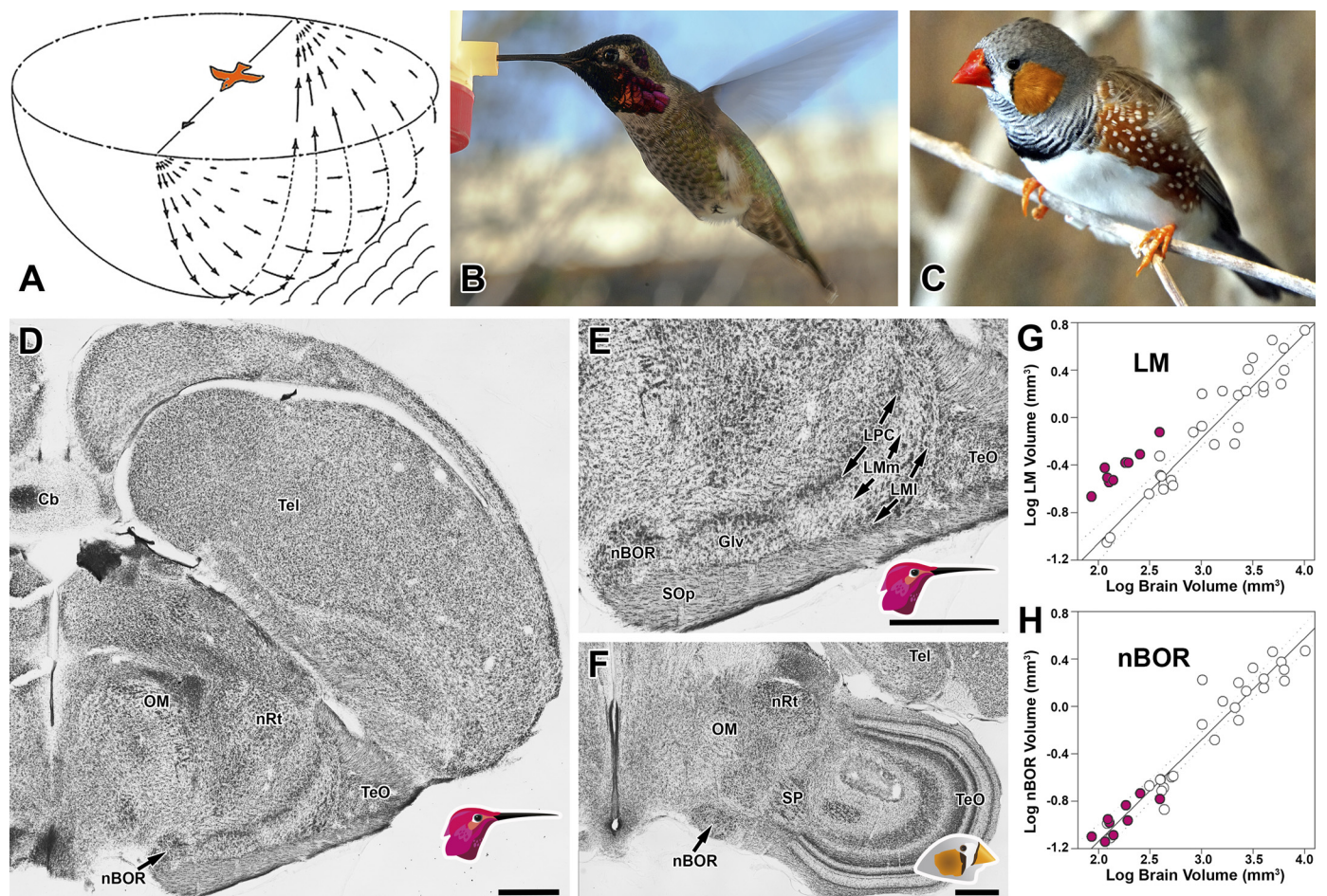
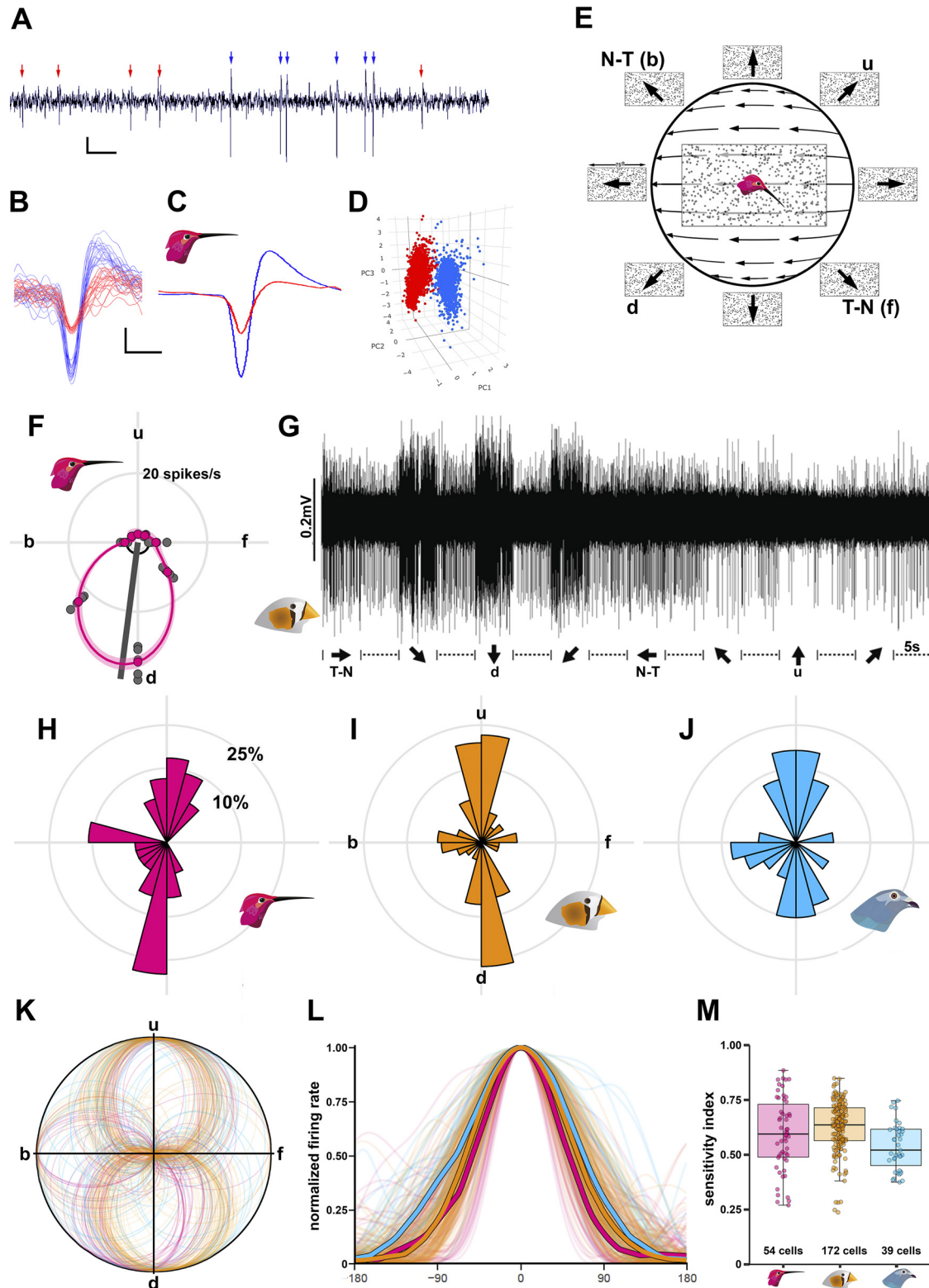


**Figure 1.** A: representation of the optic flowfield produced during forward flight (5). B: hovering Anna’s hummingbird (*Calypte anna*) (photo by T. J. Gehling; licensed under CC BY-NC-ND 2.0). C: a zebra finch (*Taeniopygia guttata*) (Dennis Jarvis, licensed under CC BY-SA 2.0). D: photomicrograph showing a Nissl-stained coronal section of hummingbird brain showing the nucleus of the basal optic root (nBOR) at the ventral surface at the level of key midbrain visual nuclei. E: higher magnification view of D showing the medial and lateral layers of the nucleus lentiformis mesencephali (LM). F: photomicrograph showing a Nissl-stained coronal section from the zebra finch at the level of the nBOR. Scatterplot depicting the log-transformed volume of the LM (G) or nBOR (H) plotted against the log-transformed brain minus LM or nBOR volume for 37 avian species. The hummingbirds are indicated by magenta circles and other species by white circles. The least-squares linear regression line is indicated for all species, and the dashed lines represent the 95% confidence interval. The hummingbird LM, but not nBOR, is hypertrophied relative to brain size. Adapted from Ref. 6. In this and subsequent figures, cartoons indicate from which species the data was obtained. Scale bars: 500  $\mu\text{m}$ . Cb, cerebellum; Giv, nucleus geniculatus lateralis, pars ventralis; LMI, lentiformis mesencephali, pars lateralis; LMm, lentiformis mesencephali, pars medialis; LPC, nucleus laminaris precommisuralis; nRt, nucleus rotundus; OM, occipitomesencephalic tract; SOP, stratum opticum; SP, nucleus subpretectalis; Tel, telencephalon; TeO, optic tectum.

pretectal nuclei have complimentary roles with respect to processing of direction of visual motion. In mammals, the medial and lateral terminal nuclei of the AOS prefer upward and downward motion, whereas neurons in the dorsal terminal nucleus of the AOS and the NOT prefer forward (i.e.,

temporal-to-nasal motion). In birds and other nonmammalian vertebrates the situation is similar, with neurons in LM preferring forward motion, whereas neurons in nBOR prefer upward, downward, and backward (i.e., nasal-to-temporal) motion (20, 23, 26–50).



The similarity of response properties of AOS and LM/NOT neurons across species from different vertebrate classes speaks to a highly conserved system. Recent data from hummingbirds, however, suggest that the system can be “specialized.” Hummingbirds are unique among birds with their ability for sustained hovering flight (Fig. 1B). A recent study showed that the exquisite stabilization during hovering flight is an optokinetic response, as hummingbirds are sensitive to small perturbations of their visual environment while hovering and drift in the direction of large-field visual motion (51). Moreover, two pieces of evidence suggests that LM has evolved to meet the demands of hovering flight. First, Iwaniuk and Wylie (6) showed that the LM is massively hypertrophied in hummingbirds: when expressed as a percentage of brain size the LM is several times larger in hummingbirds compared with other birds (Fig. 1G). Second, Gaede et al. (52) recorded from LM in hummingbirds and noted that their responses properties differed from the typical pattern. In all other previous studies of LM/NOT in tetrapods, there is a strong population bias with respect to directional tuning such that most neurons prefer temporal-to-nasal (forward) visual motion (23, 26, 29, 30, 35, 37–39, 41, 43, 46, 49, 50, 53, 54). However, hummingbirds display no bias for forward motion in the LM (52). In addition, hummingbird LM neurons were tightly tuned to faster stimulus velocities compared with that observed in zebra finches and other birds (26, 50).

If the hummingbird LM has evolved to meet the demands of hovering flight, one would also expect concomitant changes in the nBOR. We reason this because they are both involved in the analysis of optic flow (55), they both receive input from specialized retinal ganglion cells (56–58), and their information is integrated in the inferior olive and vestibulocerebellum (59–62). Although the nBOR is not hypertrophied in hummingbirds (Fig. 1H) (6), in this study we sought to determine if there were similar changes in the response properties of nBOR neurons in hummingbirds. We recorded from nBOR in both hummingbirds and zebra finches (Fig. 1, B and C) to random dot patterns varying in direction and velocity, and drifting sine-wave gratings varying in spatial and temporal frequency (SF, TF), and compared these data with archival data from pigeons (63–66). We did not find differences among the species with respect to the distribution of directions preferences of nBOR neurons as was observed in LM (52), but we did find that hummingbird neurons were more tightly tuned to stimulus velocity and in the

spatiotemporal domain. Collectively, these data suggest that both the LM and nBOR in hummingbirds are adapted to meet optokinetic demands associated with hovering flight.

## MATERIALS AND METHODS

### Animals

Sixteen adult male zebra finches (*Taeniopygia guttata*) and twelve adult male Anna’s hummingbirds (*Calypte anna*) were used for electrophysiological recording. All procedures were approved by the University of British Columbia Animal Care Committee in accordance with the guidelines set by the Canadian Council on Animal Care.

### Surgery and Electrophysiological Recording Procedures

Animals were anesthetized by intramuscular injection in the pectoralis major with a ketamine/xylazine mixture (65 mg/kg ketamine/8 mg/kg xylazine). Supplemental doses were administered as necessary. Before the surgery, a subcutaneous injection of 0.9% saline was provided for additional fluids. The nBOR is quite small and resides at the base of the brain at the mesodiencephalic border (Fig. 1, D–F). Coordinates to locate the nBOR were calculated using serial photomicrographs of fixed, Nissl-stained brain sections and a stereotaxic atlas of the zebra finch brain (Konishi, unpublished observations). Anesthetized birds were positioned in a custom-built small bird stereotaxic frame (Herb Adams Engineering, Glendora, CA). For both species, the head was positioned such that it was pitched downward 45° relative to the normal position (Fig. 2E). A small craniotomy through the skull and dura mater overlying the right telencephalon allowed access to the nBOR with vertical penetrations.

Extracellular recordings were acquired using saline-filled glass microelectrodes (2 M NaCl, 5- $\mu$ m tip diameter). The signal was amplified ( $\times 10,000$  gain; Model 3000, A-M Systems, Inc., Sequim, WA), bandpass filtered (0.1–3 kHz), sampled at 50 kHz (micro1401-3, CED; Cambridge, UK), and recorded using Spike2 for Windows (v. 8, CED; Cambridge, UK). The visual stimulus code initiated a TTL pulse from the stimulus computer to the digitizer indicating each stimulus change. Visually responsive nBOR neurons were identified, and distinguished from nearby visual nuclei, because they exhibited nonuniform excitation in response to large-field visual motion in the “preferred” direction. Typically, this was

**Figure 2.** A: representative raw recording trace showing nucleus of the basal optic root (nBOR) activity in hummingbird. Two different nBOR neurons denoted by red and blue arrows could be distinguished using the spike sorting algorithm in Spike2. B: an overlay of 20 spikes for each of the two spikes. C: an overlay of the average waveforms of both nBOR neurons (from all spikes in the entire recording). D: principal component analysis (PCA) from Spike2, illustrating that clusters from the two nBOR neuron waveforms have minimal overlap. E: to determine a cell’s preferred direction, a screen (84° horizontal  $\times$  53° vertical) was placed tangent to the retina and displayed a moving dot-field with randomly positioned black dots (2.1° diameter) on a white background, covering the entire screen. The dot-field drifted at 12.6°/s in eight directions, 45° apart. N-T, nasal-to-temporal or backward (b) motion; T-N, temporal-to-nasal or forward (f) motion. For both species, the head was pitched downward by 45°. F: a representative direction tuning curve for a hummingbird nBOR neuron. Average firing rate is plotted as a function of direction in polar coordinates. Gray dots represent the average firing in individual sweeps and the magenta dot is the mean firing rate across all sweeps in that direction. The thick magenta line is the natural cubic spline fit to the data and the shading represents the means  $\pm$  SE. The dark gray line is the preferred direction (i.e., direction of the mean vector), and the black circle represents the spontaneous rate. G: a representative recording from a zebra finch nBOR neuron in response to different directions of visual motion (arrows) interlaced with periods of no motion (dashed lines). Polar histograms show the distribution of direction preferences for all nBOR neurons recorded in hummingbirds (H), zebra finches (I), and pigeons (J). The bins are at 15° intervals. In this and subsequent figures, the data are color-coded such that magenta, orange, and blue represent hummingbirds, zebra finches, and pigeons, respectively. K: normalized (min-to-max; 0–1) tuning curves for all neurons are plotted in polar coordinates. L: normalized tuning curves aligned at the peaks. The thick lines represent the median values for the three species. M: quartile boxplots display the sensitivity index of nBOR neurons for all three species. Scale bars: A = 50  $\mu$ V, 20 ms; B and C = 50  $\mu$ V, 5 ms.

accompanied by suppression in the opposite (i.e., 180° from preferred direction), or “anti-preferred” direction.

### Offline Signal Analysis

Digitized neuronal activity was analyzed offline using Spike2 for Windows (Cambridge Electronic Design; Cambridge, UK) and MATLAB (R2017a; MathWorks; Natick, MA). Single units were classified using the spike sorting algorithm in Spike2. Spikes (wavemarks) were extracted from the raw trace using full-wave templates created using appropriate trigger thresholds to exclude noise and capture spikes. The template window was set at a width to encompass the full spike. As shown in Fig. 2, A–D, in some cases we were able to isolate two spikes at the same location. Twenty spikes overlaid from both templates identified in the signal (Fig. 2A) are shown (Fig. 2B) as well as the averages for both spike templates (Fig. 2C). These two spikes were separable with a cluster analysis of a principal component analysis (Fig. 2D).

### Visual Stimuli

After isolating a neuron, direction selectivity was initially evaluated by moving a handheld stimulus (black markings on white board) in different directions, at a range of speeds, in the contralateral visual field. Subsequently, we positioned a computer monitor (144 Hz, 1,920 × 1,080 pixels, ASUS VG248QE) within the cell’s receptive field, 30 cm away and tangent to the contralateral eye for stimulus presentation. The monitor occupied an ~84° × 53° (width × height) area of the bird’s visual field.

To test the response properties of nBOR cells, we created three visual stimulus programs using Psychophysics Toolbox-3 in MATLAB. The programs tested responses to direction, velocity, and spatiotemporal properties of visual motion. The first program was used to identify the direction preference of each cell. This was achieved by generating a plane of 250 randomly positioned black dots (2.1° diameter) on a white background, covering the entire screen. The dot field drifted at 12.6°/s in eight directions, 45° apart (Fig. 2E). Each sweep consisted of 5 s of motion, followed by a 5 s pause, in each of the eight directions (Fig. 2G), and at least four repetitions of each direction were recorded for every cell. Cumulative peristimulus time histograms (PSTHs; 20 bins) were generated for each direction of motion. A direction tuning curve was produced by plotting the mean firing rate as a function of direction in polar coordinates and fitting a natural cubic spline function to these points (Fig. 2F). We also determined the spontaneous firing rate based on the mean response during stationary visual stimulus. The mean spontaneous rate was always subtracted from the firing rate in response to a visual stimulus. To determine whether a cell was direction-sensitive, we first used Rayleigh’s test for uniformity. If a cell’s responses were nonuniform ( $P < 0.05$ ), we next calculated the preferred direction for that cell by finding the mean vector using the following equation:

$$\text{Preferred direction} = \tan^{-1} \left( \frac{\sum_n (\text{FR}_n \times \sin\theta_n)}{\sum_n (\text{FR}_n \times \cos\theta_n)} \right), \quad (1)$$

where FR = firing rate and  $n$  = the eight directions of motion in radians.

To analyze the breadth of direction tuning, we fit a cubic smoothing spline to three replicates of the complete direction tuning data set for each cell. We set the degrees of freedom for the function to all integers from 5 to 20 and compared second-order Akaike information criteria to identify the best fit for each cell. We then used the best-fit parameters to generate curves for each cell, allowing us to compare distribution of preferred directions (in polar coordinates; Fig. 2K) or to examine the sensitivity, or narrowness of the curve, for all cells (with preferred directions aligned; Fig. 2L).

A sensitivity index (SI) was also calculated for each cell as follows:

$$\text{SI} = \frac{\sqrt{(\sum_n \text{FR}_n \times \sin\theta_n)^2 + (\sum_n \text{FR}_n \times \cos\theta_n)^2}}{\sum_n \text{FR}_n}, \quad (2)$$

where  $\text{FR}_n$  is the average firing rate in response to direction  $n$  for all eight directions of motion presented (in radians). This effectively calculates the normalized length of the mean vector. The SI ranges from 0 to 1, with a higher SI indicating narrower directional tuning. An SI of 1 means that a neuron responded to a single direction of motion.

After presenting the stimuli to determine directional tuning, we presented visual stimuli using one or both of the remaining two programs (velocity and spatiotemporal tuning). To test velocity tuning, the same random dot pattern used for direction tuning was moved in the preferred direction at 12 different speeds (0.2°/s, 0.4°/s, 0.8°/s, 1.6°/s, 3.3°/s, 6.6°/s, 13.4°/s, 20.2°/s, 27.2°/s, 42.2°/s, 59.3°/s, and 79.4°/s). Each presentation of motion lasted 4 s and was followed by 4 s of a stationary random dot field. The stimuli were randomly presented without replacement (12 speeds × 2 directions × 5 repeats). All dots were moved coherently at a constant velocity.

To analyze velocity tuning, firing rates in response to motion in the preferred direction were plotted against log (velocity), and 3<sup>rd</sup>-, 4<sup>th</sup>-, 5<sup>th</sup>-, and 6<sup>th</sup>-order polynomials were fit to the data. We visually inspected each fit to determine the fit that best described the peak of the velocity tuning curve and compared models via second-order Akaike information criterion. The peak of the curve was taken as the preferred velocity for the cell. To analyze the breadth of the velocity tuning, the width of the velocity tuning curve was determined. The width was defined as the distance between the location where the rising phase crossed 50% on a min-max normalized curve and the peak value (Fig. 4, B–E). Only the rising phase was used to calculate tuning width, because in several cells, at high velocities, the velocity tuning curve plateaued or failed to return to the 50% threshold.

To test the spatiotemporal response properties of neurons, we used a visual stimulus program that generated a series of sinusoidal gratings drifting in the preferred direction with a range of spatial frequencies [SFs; 0.0155–1.0 cycles/° (cpd)] and temporal frequencies [TFs; 0.031–16 cycles/s (Hz)]. This produced 42 unique sine-wave grating patterns, which were presented in random order. Each sweep consisted of 2 s of motion followed by a 2 s pause for each pattern, and four sweeps were recorded for each SF/TF combination. Spike rates across the four sweeps were averaged for each grating

pattern and used to generate spatiotemporal contour plots (see Fig. 5).

For each cell, a variant of a two-dimensional (2-D) best-fit Gaussian function was fit to the contour plot (logarithmic scale). Spatiotemporal tuning was described by the peak and volume of this surface. The Gaussian function was defined as follows (67):

$$G(sf, tf) = A \times e^{-\frac{(\log_2(sf) - \log_2(sf_0))^2}{\sigma_{sf}^2}} \times e^{-\frac{(\log_2(tf) - \log_2(tf_p(sf)))^2}{\sigma_{tf}^2}}, \quad (3)$$

where:

$$tf_p(sf) = 2^{(Q+1) \times (\log_2(sf) - \log_2(sf_0)) + \log_2(tf_0)}, \quad (4)$$

where  $A$  is the amplitude of the Gaussian function in the  $z$ -axis, and  $sf_0$  and  $tf_0$  are the peak values of the Gaussian function. The function also requires the spatial ( $\sigma_{sf}$ ) and temporal ( $\sigma_{tf}$ ) frequency of a specific grating pattern stimulus, the spread of the Gaussian function in the spatial ( $\sigma_{sf}$ ) and temporal ( $\sigma_{tf}$ ) frequency domains, and a value for  $Q$ , the slope of the relationship between a cell's preferred velocity and spatial frequency.

Gaussian functions were fit using the solver function in Microsoft Excel and the R package `gaussplotR` (68). The values of  $sf_0$ ,  $tf_0$ ,  $\sigma_{sf}$ ,  $\sigma_{tf}$ , and  $Q$  were optimized to maximize the  $R^2$  value between the Gaussian model fit and the raw data, which correspond to each of the sine-wave gratings tested. The optimized parameters  $\sigma_{sf}$ ,  $\sigma_{tf}$ , and  $Q$  were free to take on any value but  $sf_0$  and  $tf_0$  were constrained to the tested region (i.e., 0.0155–1 cpd and 0.31–16 Hz). The optimized values for  $sf_0$  and  $tf_0$  defined the peak of the contour plot, thus the preferred SF/TF combination for the cell.

To measure the breadth of tuning in the spatiotemporal domain, we calculated the volume under the normalized Gaussian surface as

$$2 \times \Pi \times \sqrt{|\sigma_{sf}|} \times \sqrt{|\sigma_{tf}|}. \quad (5)$$

### Archival Data from Pigeons

The responses of pigeon nBOR neurons were available for direction tuning in response to drifting gratings, and spatiotemporal tuning, but not velocity tuning to random dot patterns (63–66).

### Hypothesis Testing

All statistical analyses were performed using R (v4.0.2). We used Bayesian generalized linear mixed models (69) to determine the extent to which fixed effect (species) explained variance across separate analyses of: sensitivity index, location of the velocity tuning curve peak, width of the rising interval (at 50% peak), volume under the Gaussian fit, and location of spatiotemporal peaks (on plots of temporal frequency vs. spatial frequency). For all models, the default (uninformative) prior was used. Statistical significance for a group difference was determined by assessing whether the 5%–95% credible intervals (CIs) of fixed effects overlapped.

### Histology

At the end of each experiment, we made a small dextran injection to confirm recording sites (Dextran Texas Red 3000 MW, or Dextran micro-Emerald 3000 MW, Thermo Fisher Scientific). Animals were given a lethal dose of ketamine/xylazine mixture (intramuscularly), and immediately transcardially perfused with 0.9% saline followed by 4% paraformaldehyde.

## RESULTS

### Directional Tuning

We obtained directional tuning curves from 54 hummingbird and 172 zebra finch nBOR neurons and compared these with 39 neurons from pigeon nBOR (archival data). The raw extracellular recording of a zebra finch nBOR unit in response to the eight directions of motion is shown in Fig. 2G. As is typical for optic flow sensitive neurons, the spiking rate increased to motion in some directions, and was inhibited by motion in other directions. Clearly, this unit preferred downward motion and was inhibited by upward motion. The directional tuning curve for a hummingbird nBOR neuron that preferred downward motion is shown in Fig. 2F, where average firing rate (magenta dots) is plotted as a function of direction in polar coordinates. A natural cubic spline was fit to these data (magenta line), and a preferred direction was assigned based on the direction of the mean vector (solid gray line; see MATERIALS AND METHODS).

The distribution of the preferred directions of nBOR neurons is plotted as polar histograms for hummingbirds, zebra finches, and pigeons in Fig. 2, H–J, respectively. Wylie and Frost (48) and Giovanni et al. (31) reported that nBOR neurons prefer either, upward, downward, or backward (i.e., nasal-to-temporal), whereas neurons preferring forward motion (i.e., temporal-to-nasal) were rare. The distributions from all three species indicate that they are highly similar in this regard. In all three species, the distributions of direction preferences were similar, clustering into the three groups: upward (37.0%, 44.8%, and 46.2% of nBOR neurons in hummingbirds, zebra finches, and pigeons, respectively), downward (46.3%, 41.3%, and 30.8%) and backward motion (16.7%, 9.3%, and 17.9%). Few neurons preferred forward (temporal-to-nasal) motion (0%, 4.7%, and 5.1%).

To test for species differences in the breadth of directional tuning, the directional tuning curve for each nBOR neuron was normalized to the maximum firing rate, and all were plotted in polar coordinates, color-coded by species in Fig. 2K. The three populations of neurons preferring upward, downward, and backward motion are apparent for all three species. The peaks of the normalized nBOR tuning curves were aligned in Fig. 2L. The median values for each species are shown with thick lines. Although the hummingbirds appear more tightly tuned to direction, this was not significant. In Fig. 2M, we show the sensitivity index for all neurons (see Eq. 2). Overall, direction tuning was somewhat broad, with the SI for most neurons in the range of 0.5–0.75. Although the mean SI was lowest for pigeons (~0.53), the distributions were not significant among the species.

Wylie and Frost (48) found a topographic organization in the nBOR with respect to direction preference. Neurons

preferring upward, downward, and backward motion were localized to dorsal, central, and ventrolateral regions, respectively (Fig. 3A). A similar organization with respect to upward and downward directions has been shown in chickens (27). From the present study, we have data indicating that this pattern is also apparent in hummingbirds and zebra finches. Figure 3, B–D shows the reconstruction of a single-recording track from the hummingbird nBOR where two neurons were recorded. Note that the neuron preferring upward motion was dorsal to the one preferring downward motion. In Fig. 3, E–J, tuning curves from five neurons on two adjacent recording tracks in the same coronal plane are shown. On the more medial track, No. 1, a cell preferring upward motion was dorsal to a cell preferring downward motion. On the more lateral track, No. 2, from dorsal to ventral, upward, downward, and backward cells were found in that order. In total (hummingbirds plus zebra finches), we had 20 electrode tracks where we recorded neurons with different directions (up, down, and back). In all cases, the order was one of the following: up-down (11 tracks), up-back (4 tracks), up-down-back (3 tracks), or down-back (2 tracks). Thus, we conclude that the topographic organization of nBOR is similar in the three species.

In summary, the directional tuning in the nBOR of hummingbirds is not appreciably different from pigeons or zebra

finches. This is unlike what was observed in LM, where the distribution of direction preferences was different in hummingbirds (52).

### Velocity Tuning

In response to random dot patterns drifting at twelve velocities (0.2–79.4°/s) in the preferred direction, we obtained velocity tuning from 24 and 101 nBOR neurons in hummingbirds and zebra finches, respectively. There is no comparable archival data for pigeons. Figure 4A shows a representative raw trace from a zebra finch nBOR neuron responding to random dots moving in the preferred direction at four of the velocities tested. In Fig. 4, B–E, firing rate is plotted as function of velocity and a best-fit polynomial was applied to depict the tuning curves. Two representative nBOR neurons from both hummingbirds (Fig. 4, B and C) and zebra finches (Fig. 4, D and E) are shown. The peak of the polynomial was designated as the preferred velocity and is indicated by the vertical dashed line. The preferred velocities are shown for all nBOR neurons in Fig. 4F. The distribution of velocity preferences of nBOR neurons did not differ between hummingbirds (5%–95% CI = 7.99°/s–16.70°/s) and zebra finches (8.74°/s–12.72°/s). Note that for six of the zebra finch neurons, the firing rate was maximal to the highest velocity presented (80°/s). These six neurons were assigned a

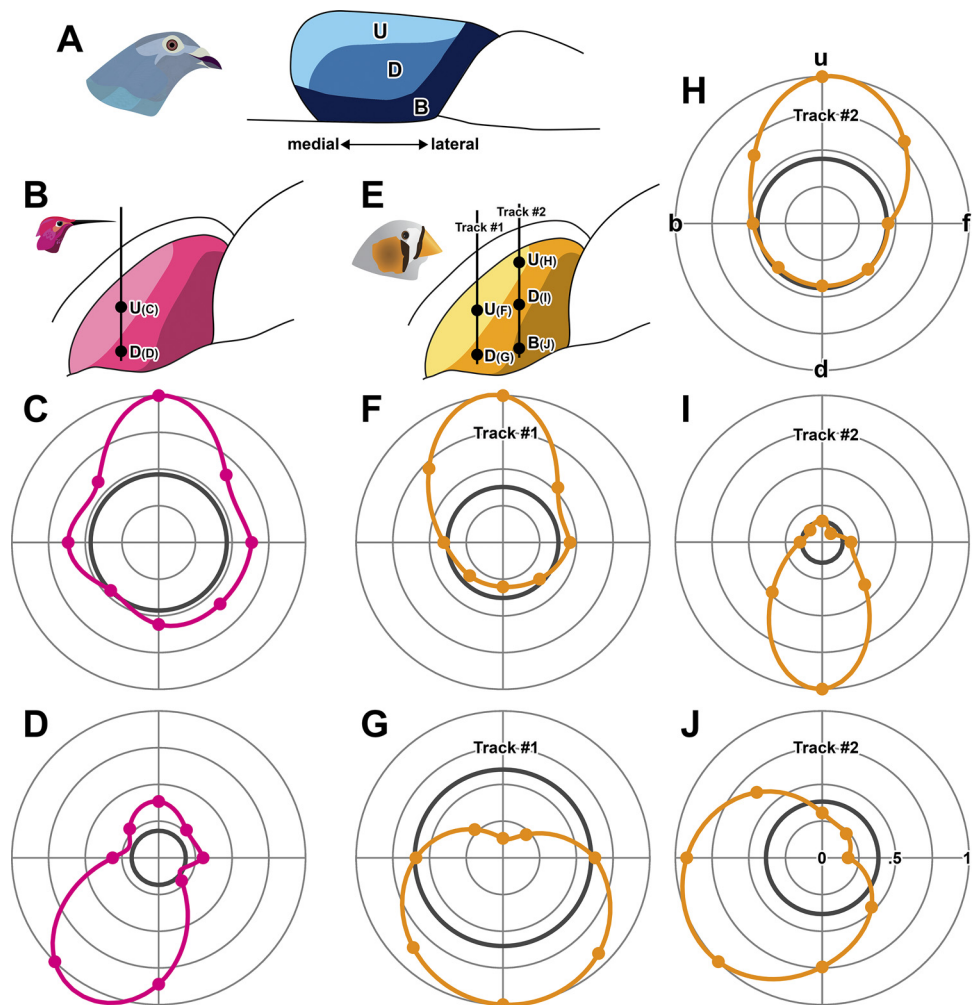


**Figure 3.** A: topography of the pigeon nucleus of the basal optic root (nBOR) (Adapted from Ref. 48). B–D: a single recording track in the hummingbird nBOR illustrating the topography of direction preferences. Direction tuning curves for two units in this track preferring upward (C) and downward (D) visual motion. E–J: tuning curves from five zebra finch nBOR units on two adjacent recording tracks in the coronal plane are shown. Direction preferences indicated in E. All tuning curves are normalized to the maximum mean firing rate for the individual cell. Nasal-to-temporal: upward (U,u), downward (D,d), and backward (B,b); temporal-to-nasal: forward (f).

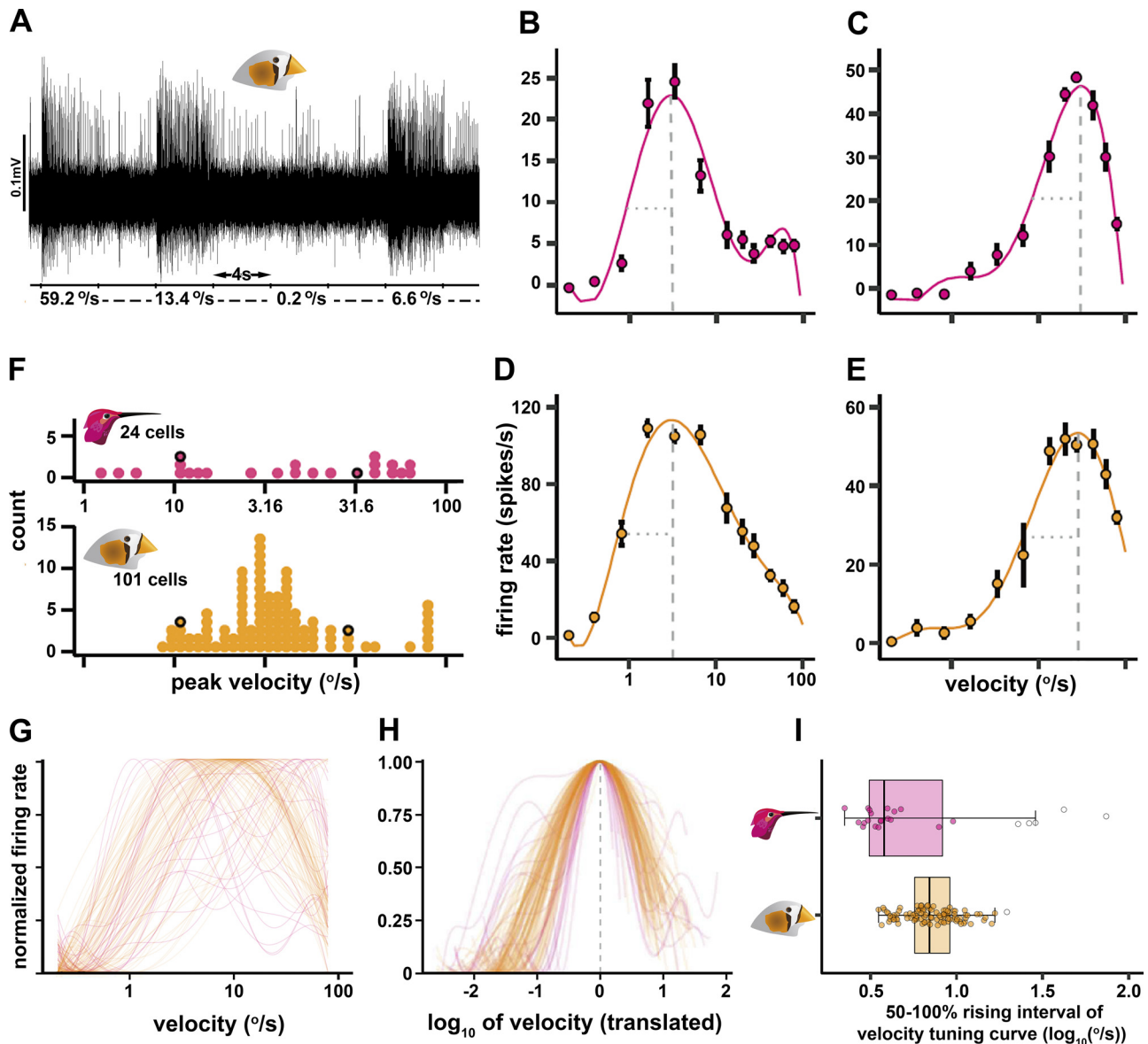


**Figure 4.** *A*: a representative raw trace depicting a zebra finch nucleus of the basal optic root (nBOR) neuron responding to a dot-field moving in the preferred direction at four different velocities. Each period of motion was separated by stationary periods (dashed lines) of the same duration (4 s). Velocity tuning curves of two hummingbird (*B* and *C*) and two zebra finch nBOR neurons (*D* and *E*); firing rate is plotted as a function of stimulus velocity and a polynomial was fit to the curve (see MATERIALS AND METHODS). The vertical and horizontal dotted lines respectively indicate peak response and 50% response level of the best-fit polynomial. *F*: the distributions of velocity preferences are similar for hummingbird and zebra finch nBOR neurons. The black circles represent the peaks from the tuning curves depicted in each of *B–E*. *G–I*: an analysis of velocity tuning curves indicates that nBOR neurons are more narrowly tuned to velocity in hummingbirds than in zebra finches. Normalized tuning curves for all neurons are plotted as a function of stimulus velocity (*G*). These tuning curves were aligned at the peaks (*H*). A quartile boxplot (*I*) displays the width in  $^{\circ}/s$  of the 50%–100% rising interval of the velocity tuning curves (i.e., dotted horizontal lines in *B–E*). There were six zebra finch neurons in which the firing rate was highest to the maximum stimulus velocity used. The peak velocity was designated as  $80^{\circ}/s$  in *F*, but these cells were not included in the analysis of tuning width in *G–I*.

preferred velocity of  $80^{\circ}/s$ , but note that these values may be underestimates.

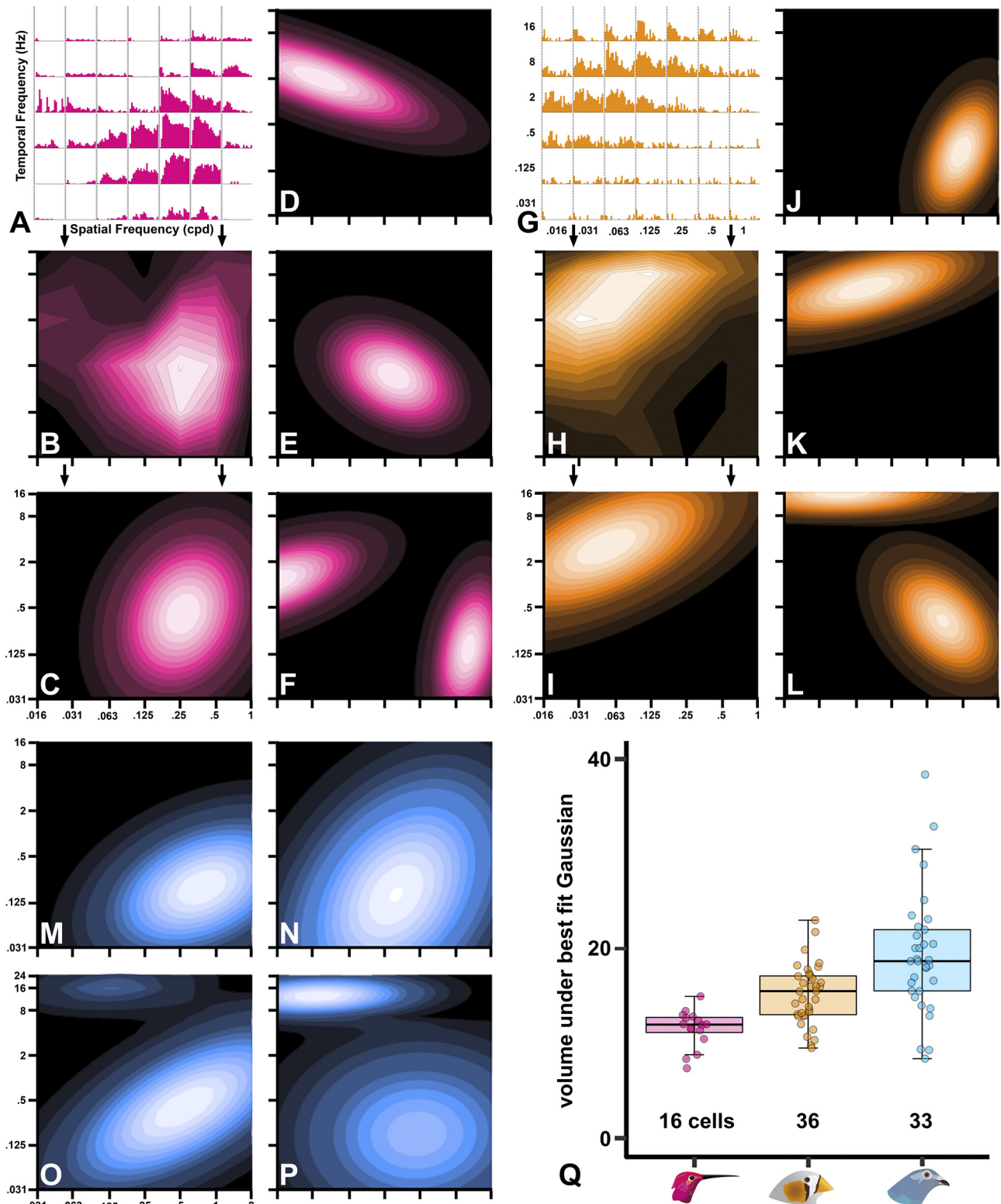
To examine the breadth of velocity tuning, we first plotted normalized velocity response curves for all nBOR neurons (Fig. 4*G*) and aligned the peaks of the best-fit polynomials (Fig. 4*H*). The six zebra finch neurons that showed maximal firing to  $80^{\circ}/s$  were not included in this analysis. In Fig. 4*H*, the peaks of the polynomials were aligned, and the hummingbird neurons appeared to be more tightly tuned. This was quantified using the width

of the 50%–100% rising interval of the velocity tuning curve, which is indicated by the dotted horizontal lines in the representative tuning curves (Fig. 4, *B–E*). Shown with quartile box plots in Fig. 4*I*, the width of the rising interval was lower for nBOR neurons of hummingbirds (5%–95% CI:  $0.50 \log^{\circ}/s$ – $0.64 \log^{\circ}/s$ ) compared with that of zebra finches (5%–95% CI:  $0.82 \log^{\circ}/s$ – $0.88 \log^{\circ}/s$ ). These nonoverlapping CIs indicated a statistically significant group difference between species. Six cells, indicated by the open circles, were statistical outliers and

therefore not included in the credible intervals. These few neurons were very broadly tuned, and some had multiple peaks in the 50%–100% rising interval.

In summary, the velocity preferences of hummingbird nBOR neurons were not different from that of zebra finches. This is

unlike what was previously found in the LM: in hummingbirds, LM neurons preferred faster velocities compared with zebra finches (52). We did find that hummingbird nBOR neurons were more tightly tuned to velocity compared with zebra finches, consistent with what was previously found for LM (52).



## Responses to Drifting Sine-Wave Gratings

We measured the responses of 16 and 36 nBOR neurons in hummingbirds and zebra finches, respectively, to sine-wave gratings drifting in the preferred direction. These data were compared with 33 nBOR neurons from archival pigeon data (50, 63–65). We used temporal frequencies (TFs) in the range of 0.031–16 Hz. This was the range used for the majority of neurons in the pigeon studies, but some neurons were exposed to stimuli at 24 Hz (see Fig. 5, *O* and *P*). The range of spatial frequencies (SFs) used in the pigeon studies was 0.031–2 cpd. In our initial recordings from the hummingbird nBOR, we noted that some cells responded vigorously to the lowest spatial frequency used, so we shifted the SF range by one log unit (0.0155–1 cpd). The range of velocity of the stimuli was  $0.031^\circ/\text{s}$ – $1032^\circ/\text{s}$  (velocity = TF/SF). Representative responses to sine-wave gratings moving in the preferred direction are shown for individual hummingbird and zebra finch neurons in Fig. 5, *A–C* and Fig. 5, *G–I*, respectively. In Fig. 5, *A* and *G*, peristimulus time histograms (PSTHs) for each combination of SF and TF are presented. Each PSTH is averaged over four sweeps and only the 2-s epoch where the moving stimulus was presented is shown. A contour plot of these data for each species is shown in Fig. 5, *B* and *H*, and the best-fit Gaussian is depicted in Fig. 5, *C* and *I*. The best-fit Gaussians for three other nBOR cells from hummingbirds (Fig. 5, *D–F*), and zebra finches (Fig. 5, *J–L*) are also shown, along with four such plots from the pigeon data (Fig. 5, *M–P*). Note that in all species, some neurons had two peak response regions in the spatiotemporal domain, although of different magnitudes (Fig. 5, *F*, *L*, *O*, and *P*). This has also been observed for some optic flow neurons in the wallaby (37).

In the contour plots in Fig. 5, the hummingbird nBOR neurons appear more tightly tuned in the spatiotemporal domain. We quantified tuning specificity for the best-fit Gaussians for all nBOR neurons by calculating the volume under the Gaussian fit (see Eq. 5, MATERIALS AND METHODS; units = log Hz  $\times$  log cpd). For the neurons that had two peaks, only the volume of the peak with the higher magnitude was measured (mean values for Gaussian volumes were similar after removing cells with two peaks; all cells: hummingbird = 11.66, zebra finch = 16.12, pigeon = 20.50; cells with one peak only: hummingbird = 11.61, zebra finch = 16.10, pigeon = 20.60). Figure 5*Q* shows a quartile boxplot of these data. The hummingbird nBOR neurons (5%–95% CI = 8.97–13.37) are more tightly tuned in the spatiotemporal domain compared with zebra finch neurons (5%–95% CI = 13.62–16.78), which are more tightly tuned than pigeon neurons (5%–95% = 17.74–20.93). These nonoverlapping CIs indicated statistically significant differences between species.

The peak of the best-fit Gaussian was designated as the preferred SF/TF combination for each cell, and these are plotted in Fig. 6*A*. In cases where the peak SF or TF had to be constrained to the range of SFs and TFs that we used, an open circle is plotted. It is possible that the actual peak response lies beyond the range we tested. The kernel density estimates for the SF, TF, and velocity (i.e., TF/SF) are plotted above, to the right, and in the upper right, respectively. Previous reports found that NOT neurons in wallabies (37), LM neurons in pigeons (50), and nBOR neurons in pigeons (66) are divided into two groups: those that preferred low SFs and high TFs and those that preferred high SFs and low TFs. As velocity is equal to TF/SF, these groups were referred to as “fast” and “slow” cells. A cluster analysis supported the distinction of fast and slow groups in the present study. The boundary between the groups is at  $8^\circ/\text{s}$  (solid line in Fig. 6*A*).

The credible intervals for effect sizes of velocity, SF, and TF for nBOR neurons are shown in Fig. 6, *B–D* for the fast cells and in Fig. 6, *E–G* for the slow cells. In the hummingbird nBOR, the slow cells preferred faster velocities compared with zebra finches and pigeons (Fig. 6*E*). This result was due to a preference for markedly lower SFs (Fig. 6*F*). There were no differences in the velocity preferences of the fast cells, although hummingbird nBOR neurons preferred lower SFs (Fig. 6*C*). There were some modest differences in TF, with the slow nBOR cells of pigeons preferring lower TFs than hummingbirds (Fig. 6*G*), and the fast nBOR cells of zebra finches preferring higher TFs than hummingbirds (Fig. 6*D*).

## DISCUSSION

This study was motivated by a previous study examining the responses of LM neurons in hummingbirds to large-field motion (52). Compared with zebra finches and pigeons, LM neurons of hummingbirds differed in several respects and it was postulated that these changes represented adaptations to meet the demands of hovering flight in hummingbirds (6, 51, 70). We reasoned that if the LM has adapted to meet the demands of hovering flight, concomitant changes might also be seen in the hummingbird nBOR. As outlined below, we show that neurons in the hummingbird nBOR differ from other birds in only a few aspects.

### Direction Tuning

Gaede et al. (52) found that the direction preferences of hummingbird LM neurons differed from that of other birds, indeed all other tetrapods studied. Whereas there was a strong directional bias toward forward (i.e., temporal-to-nasal) motion in the LM of zebra finches and pigeons (26, 49, 50), no such bias was observed in the distribution of direction preferences in the hummingbird LM. This was quite

**Figure 5.** Responses of nucleus of the basal optic root (nBOR) neurons to drifting sine-wave gratings. *A*: peristimulus time histograms showing responses of a representative hummingbird nBOR neuron to drifting sine-wave gratings of varying temporal and spatial frequency. Each histogram shows the average spike rate for four repetitions of the same stimulus divided into 100 ms time-bins over 2 s of stimulus motion. *B*: the same data from *A* are represented by a contour plot with firing rate indicated by color. The data are normalized and white indicates peak firing (100%), with progressively darker colors indicating less firing in equal increments (black = 0%). *C*: the contour plot from *B* is fit with a two-dimensional Gaussian. *D–F*: best-fit Gaussians for the firing profiles of three other hummingbird nBOR neurons. *G*: peristimulus time histograms showing spatiotemporal responses of a representative zebra finch nBOR neuron to drifting sine-wave gratings (as described for *A*). *H*: the same data in *G* are represented by a contour plot with firing rate indicated by color. *I*: the contour plot from *H* is fit with a two-dimensional Gaussian. *J–L*: best-fit Gaussians for the firing profiles of three other zebra finch nBOR neurons. *M–P*: best-fit Gaussians for the firing profiles of four pigeon nBOR neurons. *Q*: boxplots of the volume under the Gaussian fits (see Eq. 5 in MATERIALS AND METHODS) indicate that hummingbird nBOR neurons are more tightly tuned in the spatiotemporal domain. See text for additional details.

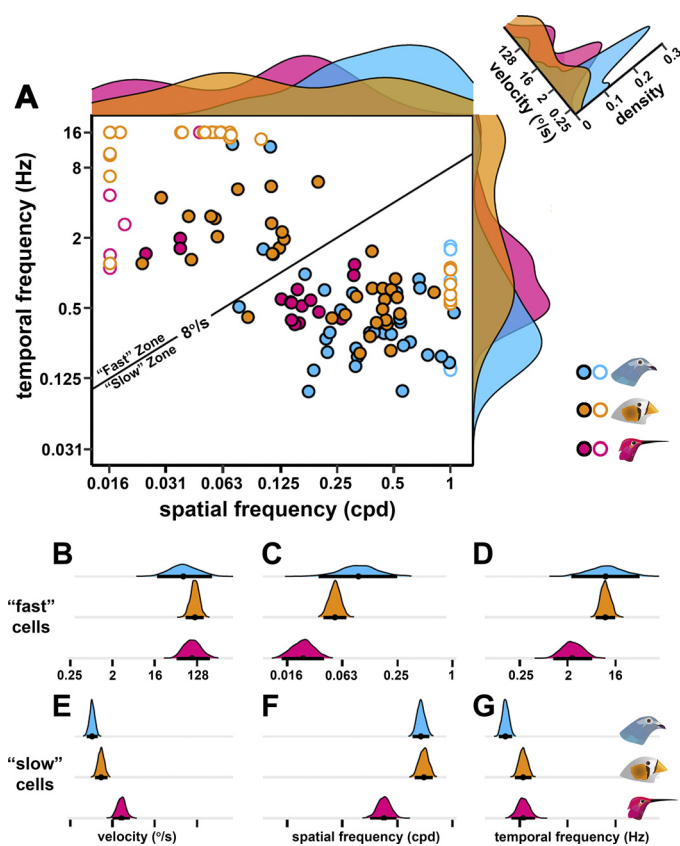


**Figure 6.** A: the locations of the peaks of the unconstrained best-fit Gaussians to all nucleus of the basal optic root (nBOR) neurons are plotted for hummingbirds (magenta), zebra finches (orange), and pigeons (light blue). For neurons with two peaks, only the location of the larger peak is depicted. Open circles indicate that the fitted Gaussians were found to peaks at or beyond the edge of the ranges of spatial frequencies (SFs) and temporal frequencies (TFs) used. (i.e., the Gaussian was constrained to the tested region). A cluster analysis separated the nBOR neurons into “fast” ( $>8^\circ/\text{s}$ ) and “slow” groups, as indicated by the solid black line. Kernel density estimates for the SF, TF, and velocity are plotted *top*, to the *right*, and in the *top right*, respectively. B–D: distributions of species’ effects in models of velocity, SF, and TF for “fast” nBOR neurons. In each panel, the species’ mean effect is indicated by the black dot, whereas the 5%–95% credible interval (CI) is shown using a black bar. E–G: distributions of species’ effects (with mean and 5%–95% CI) for “slow” nBOR cells.

surprising given that the bias toward forward motion is apparent in the LM/NOT of all tetrapods (23, 29, 30, 35, 37–39, 41, 43, 46, 53, 54). This lack of a bias in hummingbirds was thought to reflect the fact that hovering hummingbirds show optokinetic drift to stimuli moving in all directions (51), whereas in most animals the optokinetic response is stronger to temporal-to-nasal motion (e.g., see Refs. 71 and 72).

Unlike that observed in the LM, the direction tuning in the hummingbird nBOR does not appear to be different from other birds. At the population level, direction preferences in the pigeon nBOR are complimentary to those observed in LM, as nBOR neurons prefer upward, downward, and backward motion, and neurons preferring forward motion are rare (31, 48). In both hummingbirds and zebra finches, the distribution of direction preferences matched what had been

observed in pigeons (Fig. 2, H–J). The species also did not differ with respect to the breadth of tuning (Fig. 2, K and L), although LM neurons did not show differences in this regard (52, 70). Finally, the topography of the nucleus with respect to direction is strikingly similar in all three species (Fig. 3).

### Velocity Tuning

Upon observing that the LM was hypertrophied in hummingbirds, Iwaniuk and Wylie (6) suggested that this was due to enhance the optokinetic response to support the exquisite head stabilization observed during hovering flight. Specifically, they suggested that most cells would be tuned to slow velocities, thus minimizing the slightest retinal slip. Iwaniuk and Wylie (6) could not have been more wrong, as Gaede et al. (52) found that the distribution of velocity preferences was skewed to very high velocities. This suggests that hypertrophy of LM is to increase the performance of the optokinetic response at the onset to stimulus motion, when retinal slip velocities are very high (37).

In the present study, we did not find any species differences in the distribution of velocity preferences of nBOR neurons in response to random dot stimuli drifting in the preferred direction up to  $80^\circ/\text{s}$ . Gaede et al. (52) also found that LM neurons were more tightly tuned in hummingbird neurons compared with zebra finches. We found that this is also the case for nBOR neurons in hummingbirds (Fig. 4, H and I). Thus, although the nBOR did not show difference in the preferred speed for visual motion as was observed in LM, optic flow neurons in both nuclei are relatively tightly tuned to stimulus velocity.

### Spatiotemporal Tuning

In the present study, we also examined the responses of hummingbird and zebra finch LM neurons to sine-wave gratings of varying SF and TF drifting in the preferred direction. The use of these stimuli allowed us to extend the upper end of the velocity range with the use of low SFs drifting at high TFs. Ibbotson et al. (37) found that the neurons in the NOT of wallabies were separated into “slow” versus “fast” groups based on their preference for high SFs and low TFs versus low SFs and high TFs. Wylie and Crowder (50) found the same groupings in pigeons, first for LM neurons (73) and subsequently for nBOR (64, 66). In the present study, we confirmed the distinction between “fast” and “slow” groups for nBOR neurons in both hummingbirds and zebra finches (Fig. 6). Although the proportion of fast cells was rather low for the pigeon sample (Fig. 6A), in previous studies this has been higher (50, 64). We did observe some species differences but of rather modest magnitude: the hummingbird nBOR slow and fast neurons preferred slightly lower SFs, and the slow cells preferred slightly faster velocities compared with zebra finches and pigeons (Fig. 6, C, E, and F).

A more dramatic species difference was seen with respect to the breadth of tuning in the spatiotemporal domain. nBOR neurons in hummingbirds were much more tightly tuned compared with zebra finches and hummingbirds (Fig. 5Q). Most of the hummingbird neurons were responding to only a few of the 42 stimuli presents (Fig. 5, D–F). These data

mirror the tight velocity tuning of hummingbird LM (52) and nBOR neurons (Fig. 4) to random dot patterns.

### Adaptive Specialization of the Highly Conserved Brainstem Optic Flow Pathways

Among Jerry Simpson's most notable contributions was the demonstration that the optic flow and vestibular systems share a common three-axis reference frame. In the inferior olive, and reflected in the complex spike activity of floccular Purkinje cells, visually responsive neurons respond best to rotational optic flow about either the vertical axis, or one of two horizontal axes that are oriented 45° to the midline (3, 4). These are the same three axes that result in maximal stimulation of the vestibular canals (13). This is also the reference frame of the extraocular muscles: i.e., pairs of extraocular muscles rotate the eye about the vertical axis, or one of two horizontal axes oriented 45° to the midline, despite different placements of the eye within the orbit across mammalian species (74–76). Furthermore, Jerry recognized that a bias toward this reference frame is present in the direction preferences of the ON-type ganglion cells in the retina described by Oyster (77) and the retinal recipient nuclei of the AOS (1).

Wylie and Frost (49, 78–80) showed that the visual signals to the pigeon flocculus also encode the visual consequences of self-rotation with the same spatial reference frame as that of the semicircular canals and eye muscles, emphasizing that this relationship is highly conserved in the AOS/pretectal-olivo-vestibulocerebellar pathways in vertebrates. These pathways exhibit conservation of several other key properties (18, 21, 24, 25, 81, 82). For example, Ibbotson and Price (73) noted that the NOT in wallabies and the LM in pigeons both contain “fast” cells that prefer low SFs drifting at high TFs and “slow” cells that prefer high SFs drifting at low TFs (37, 50). Such fast and slow cells are also seen in the nBOR of pigeons (66), and the present study shows that this is the case for the nBOR in hummingbirds and zebra finches.

Given that a wealth of data speaks to conservation within the brainstem optic flow pathways across vertebrates, it is somewhat surprising that we observe differences between species of birds and specialization within hummingbirds. We contend that these systems have undergone numerous adaptive changes to support the optokinetic demands of hovering flight (70). The ability to precisely encode the speed and direction of optic flow is a key feature that allows these small birds to hover, maneuver, and feed on the wing in dense foliage. It appears that more changes have occurred in the pretectum as opposed to the AOS, consistent with the fact that the LM is hypertrophied in hummingbirds, but the nBOR is not (6) (Fig. 1, G and H). The LM has undergone changes with respect to direction tuning and a preference for faster velocities (52). Neurons in both the LM and nBOR of hummingbirds show tighter tuning to stimulus velocity measured with both random dot patterns and gratings varying in SF and TF (Figs. 4 and 5). We have argued elsewhere (5, 83) that the hummingbird could be regarded as a visual “velocity specialist” forgoing a coarse or population code common in perceptual systems (84) for a “specificity” or “sparse” code (85) seen in other sensory specialists. For example, owls are auditory specialists with a hypertrophied

inferior colliculus containing neurons tightly tuned for auditory space (86–89). With a sparse code, as the neurons are more tightly tuned to a particular stimulus dimension, relatively few neurons are activated in response to a stimulus (90). The cost is that more neurons are required to cover range of that stimulus dimension, which carries a high energy demand (91).

But how has the circuitry changed in hummingbirds to account for the adaptive responses to optic flow? It is possible that the retinal inputs themselves have changed, but these appear highly similar in pigeons, hummingbirds, and zebra finches (56, 58). More likely, the velocity and directional tuning may be altered by inputs from the visual “Wulst,” a telencephalic structure homologous to striate cortex (92). The Wulst projects to both the nBOR and LM in pigeons (93–96) but this projection has not been studied in hummingbirds. A telencephalic projection from visual cortical areas to the NOT and AOS has been shown in several mammalian species [e.g., cats and monkeys (97–103), rats (104), guinea pigs (105), and rabbits (106)]. Grasse and Cynader (98) have outlined how the AOS has been adaptively modified in frontally eyed mammals to meet the demands associated with binocular vision. Modifications include binocular as opposed to monocular-contralateral receptive fields, responsiveness to faster velocities, and some changes in the distribution of direction preferences. These adaptive modifications are clearly due to cortical afferents, as after lesions to visual cortical areas, the receptive fields of neurons in the LM and AOS are monocular, do not respond to faster velocities, and show a distribution of direction preferences like that observed in lateral-eyed mammals (107, 108); see also Refs. 99 and 109. Given these data, we speculate that, in hummingbirds, the tighter tuning to stimulus velocity in nBOR and LM, the shift toward a preference to faster velocities in LM, and the changes in the distribution of direction preferences in LM may be due to afferents from the visual Wulst.

### Conclusions

The AOS and pretectal pathways responsible for the analysis of optic flow and the generation of the optokinetic response are regarded as highly conserved across tetrapod vertebrates (11, 18, 21, 24, 25, 82). Data from hummingbirds, however, suggest that these systems have undergone numerous adaptive changes to support the optokinetic demands of hovering flight. The ability to precisely encode the speed and direction of optic flow is a key feature that allows these small birds to hover, maneuver, and feed on the wing in dense foliage. It appears that more changes have occurred in the pretectum as opposed to the AOS, consistent with the fact that LM is hypertrophied in hummingbirds, but the nBOR is not (6) (Fig. 1, G and H). The LM has undergone changes with respect to direction tuning and a preference for faster velocities (52). Neurons in both the LM and nBOR show tighter tuning to stimulus velocity. These data suggest a potentially rich, untapped data set of species-specific specializations in optic flow analysis related to environment. Further study examining species living in distinct habitats or with specialized modes of locomotion may elucidate neural processing algorithms that support maneuverability or navigation through complex environments.

## ACKNOWLEDGMENTS

The acknowledgment for the hovering hummingbird photograph in the graphical abstract should be Anand Varna.

## GRANTS

This research was supported by funding from the Canadian Institute for Health Research (CIHR) and Natural Sciences and Engineering Research Council of Canada (NSERC) (to D.L.A. and D.R.W.).

## DISCLOSURES

No conflicts of interest, financial or otherwise, are declared by the authors.

## AUTHOR CONTRIBUTIONS

A.H.G., G.S., D.L.A., and D.R.W. conceived and designed the research; A.H.G. and G.S. performed experiments; A.H.G., V.B.B., G.S., C.G.-I., D.L.A., and D.R.W. analyzed data; A.H.G., V.B.B., G.S., C.G.-I., D.L.A., and D.R.W. interpreted results of experiments; A.H.G., V.B.B., G.S., C.G.-I., D.L.A., and D.R.W. prepared figures; A.H.G., V.B.B., G.S., C.G.-I., D.L.A., and D.R.W. drafted manuscript; A.H.G., V.B.B., G.S., C.G.-I., D.L.A., and D.R.W. edited and revised manuscript; A.H.G., V.B.B., G.S., C.G.-I., D.L.A., and D.R.W. approved final version of manuscript.

## REFERENCES

- Soodak RE, Simpson JI. The accessory optic system of rabbit. I. Basic visual response properties. *J Neurophysiol* 60: 2037–2054, 1988. doi:10.1152/jn.1988.60.6.2037.
- Simpson JI, Leonard CS, Soodak RE. The accessory optic system of rabbit. II. Spatial organization of direction selectivity. *J Neurophysiol* 60: 2055–2072, 1988. doi:10.1152/jn.1988.60.6.2055.
- Leonard CS, Simpson JI, Graf W. Spatial organization of visual messages of the rabbit's cerebellar flocculus. I. Typology of inferior olive neurons of the dorsal cap of Kooy. *J Neurophysiol* 60: 2073–2090, 1988. doi:10.1152/jn.1988.60.6.2073.
- Graf W, Simpson JI, Leonard CS. Spatial organization of visual messages of the rabbit's cerebellar flocculus. II. Complex and simple spike responses of Purkinje cells. *J Neurophysiol* 60: 2091–2121, 1988. doi:10.1152/jn.1988.60.6.2091.
- Wylie DR, Gutiérrez-Ibáñez C, Gaede AH, Altshuler DL, Iwaniuk AN. Visual-cerebellar pathways and their roles in the control of avian flight. *Front Neurosci* 12: 223, 2018. doi:10.3389/fnins.2018.00223.
- Iwaniuk AN, Wylie DR. Neural specialization for hovering in hummingbirds: hypertrophy of the pretectal nucleus lentiformis mesencephali. *J Comp Neurol* 500: 211–221, 2007. doi:10.1002/cne.21098.
- Gibson JJ. The visual perception of objective motion and subjective movement. *Psychol Rev* 61: 304–314, 1954. doi:10.1037/h0061885.
- Waespe W, Henn V. Gaze stabilization in the primate. The interaction of the vestibulo-ocular reflex, optokinetic nystagmus, and smooth pursuit. *Rev Physiol Biochem Pharmacol* 106: 37–125, 1987.
- Westheimer G, McKee SP. Visual acuity in the presence of retinal-image motion. *J Opt Soc Am* 65: 847–850, 1975. doi:10.1364/JOSA.65.000847.
- Nakayama K. Differential motion hyperacuity under conditions of common image motion. *Vision Res* 21: 1475–1482, 1981. doi:10.1016/0042-6989(81)90218-2.
- Simpson JI. The accessory optic system. *Annu Rev Neurosci* 7: 13–41, 1984. doi:10.1146/annurev.ne.07.030184.000305.
- Marg E. Neurophysiology of the accessory optic system. In: *Visual Centers in the Brain*, edited by Berlucchi G, Brindley GS, Brooks B, Creutzfeldt OD, Dodt E, Doty RW, Freund H-J, Gross CG, Jeffreys DA, Jung R, Kuhnt U, MacKay DM, Marg E, Negrão N, Rizzolatti G, Sprague JM, Székely G, Szentágothai J, Whitteridge D, Jung R. Berlin: Springer, 1973, p. 103–111.
- Simpson JI, Soodak RE, Hess R. The accessory optic system and its relation to the vestibulocerebellum. *Prog Brain Res* 50: 715–724, 1979. doi:10.1016/S0079-6123(08)60868-7.
- Hubel DH, Wiesel TN. Receptive fields, binocular interaction and functional architecture in the cat's visual cortex. *J Physiol* 160: 106–154, 1962. doi:10.1113/jphysiol.1962.sp006837.
- Frost BJ, DiFranco DE. Motion characteristics of single units in the pigeon optic tectum. *Vision Res* 16: 1229–1234, 1976. doi:10.1016/0042-6989(76)90046-8.
- Hobbelen JF, Collewijn H. Effect of cerebro/cortical and collicular ablations upon the optokinetic reactions in the rabbit. *Doc Ophthalmol* 30: 227–236, 1971. doi:10.1007/BF00142521.
- Lazar G. Role of the accessory optic system in the optokinetic nystagmus of the frog. *Brain Behav Evol* 5: 443–460, 1972. doi:10.1159/000123761.
- Giolli RA, Blanks RHI, Lui F. The accessory optic system: basic organization with an update on connectivity, neurochemistry, and function. *Prog Brain Res* 151: 407–440, 2006. doi:10.1016/S0079-6123(05)51013-6.
- Brecha N, Karten HJ, Hunt SP. Projections of the nucleus of the basal optic root in the pigeon: an autoradiographic and horseradish peroxidase study. *J Comp Neurol* 189: 615–670, 1980. doi:10.1002/cne.901890404.
- Rosenberg AF, Ariel M. Visual-response properties of neurons in turtle basal optic nucleus in vitro. *J Neurophysiol* 63: 1033–1045, 1990. doi:10.1152/jn.1990.63.5.1033.
- Fite KV. Pretectal and accessory-optic visual nuclei of fish, amphibia and reptiles: theme and variations. *Brain Behav Evol* 26: 71–90, 1985. doi:10.1159/000118769.
- Collewijn H. Oculomotor areas in the rabbits midbrain and pretectum. *J Neurobiol* 6: 3–22, 1975. doi:10.1002/neu.480060106.
- Hoffmann K-P, Schoppmann A. A quantitative analysis of the direction-specific response of neurons in the cat's nucleus of the optic tract. *Exp Brain Res* 42: 146–157, 1981. doi:10.1007/BF00236901.
- Gamlin PDR. The pretectum: connections and oculomotor-related roles. *Prog Brain Res* 151: 379–405, 2006. doi:10.1016/S0079-6123(05)51012-4.
- McKenna OC, Wallman J. Accessory optic system and pretectum of birds: comparisons with those of other vertebrates (part 1 of 2). *Brain Behav Evol* 26: 91–103, 1985. doi:10.1159/000118770.
- Winterson BJ, Brauth SE. Direction-selective single units in the nucleus lentiformis mesencephali of the pigeon (*Columba livia*). *Exp Brain Res* 60: 215–226, 1985. doi:10.1007/BF00235916.
- Burns S, Wallman J. Relation of single unit properties to the oculomotor function of the nucleus of the basal optic root (accessory optic system) in chickens. *Exp Brain Res* 42: 171–180, 1981. doi:10.1007/BF00236903.
- Cochran SL, Dieringer N, Precht W. Basic optokinetic-ocular reflex pathways in the frog. *J Neurosci* 4: 43–57, 1984. doi:10.1523/JNEUROSCI.04-01-00043.1984.
- Collewijn H. Direction-selective units in the rabbit's nucleus of the optic tract. *Brain Res* 100: 489–508, 1975. doi:10.1016/0006-8993(75)90154-7.
- Fan TX, Weber AE, Pickard GE, Faber KM, Ariel M. Visual responses and connectivity in the turtle pretectum. *J Neurophysiol* 73: 2507–2521, 1995. doi:10.1152/jn.1995.73.6.2507.
- Gioanni H, Rey J, Villalobos J, Dalbera A. Single unit activity in the nucleus of the basal optic root (nBOR) during optokinetic, vestibular and visuo-vestibular stimulations in the alert pigeon (*Columba livia*). *Exp Brain Res* 57: 49–60, 1984. doi:10.1007/BF00231131.
- Grasse KL, Cynader MS. Electrophysiology of medial terminal nucleus of accessory optic system in the cat. *J Neurophysiol* 48: 490–504, 1982. doi:10.1152/jn.1982.48.2.490.
- Grasse KL, Cynader MS. Electrophysiology of lateral and dorsal terminal nuclei of the cat accessory optic system. *J Neurophysiol* 51: 276–293, 1984. doi:10.1152/jn.1984.51.2.276.
- Gruberg ER, Grasse KL. Basal optic complex in the frog (*Rana pipiens*): a physiological and HRP study. *J Neurophysiol* 51: 998–1010, 1984. doi:10.1152/jn.1984.51.5.998.
- Hoffmann KP, Distler C, Erickson RG, Mader W. Physiological and anatomical identification of the nucleus of the optic tract and dorsal

- terminal nucleus of the accessory optic tract in monkeys. *Exp Brain Res* 69: 635–644, 1988. doi:10.1007/BF00247315.
36. Hoffmann K-P, Schoppmann A. Retinal input to direction selective cells in the nucleus tractus opticus of the cat. *Brain Res* 99: 359–366, 1975. doi:10.1016/0006-8993(75)90037-2.
  37. Ibbotson MR, Mark RF, Maddess TL. Spatiotemporal response properties of direction-selective neurons in the nucleus of the optic tract and dorsal terminal nucleus of the wallaby, *Macropus eugenii*. *J Neurophysiol* 72: 2927–2943, 1994. doi:10.1152/jn.1994.72.6.2927.
  38. Katte O, Hoffmann K-P. Direction specific neurons in the pretectum of the frog (*Rana esculenta*). *J Comp Physiol* 140: 53–57, 1980. doi:10.1007/BF00613747.
  39. Li Z, Fite KV, Montgomery NM, Wang SR. Single-unit responses to whole-field visual stimulation in the pretectum of *Rana pipiens*. *Neurosci Lett* 218: 193–197, 1996. doi:10.1016/S0304-3940(96)13117-7.
  40. Manteuffel G. The accessory optic system in the newt, triturus cristatus: unitary response properties from the basal optic neuropil. *Brain Behav Evol* 21: 175–184, 1982. doi:10.1159/000121625.
  41. Manteuffel G. Electrophysiology and anatomy of direction-specific pretectal units in *Salamandra*. *Exp Brain Res* 54: 415–425, 1984. doi:10.1007/BF00235466.
  42. Morgan B, Frost BJ. Visual response characteristics of neurons in nucleus of basal optic root of pigeons. *Exp Brain Res* 42: 181–188, 1981. doi:10.1007/BF00236904.
  43. Natal CL, Britto LRG. The pretectal nucleus of the optic tract modulates the direction selectivity of accessory optic neurons in rats. *Brain Res* 419: 320–323, 1987. doi:10.1016/0006-8993(87)90600-7.
  44. Natal CL, Britto LRG. The rat accessory optic system: effects of cortical lesions on the directional selectivity of units within the medial terminal nucleus. *Neurosci Lett* 91: 154–159, 1988. doi:10.1016/0304-3940(88)90760-4.
  45. Rojas X, Marín G, Wallman J. Novel, continuous visual motion induces c-fos expression in the avian optokinetic nuclei and optic tectum. *Neuroscience* 160: 540–554, 2009. doi:10.1016/j.neuroscience.2009.02.018.
  46. Volchan E, Rocha-Miranda CE, Picanço-Diniz CW, Zinsmeister B, Bernardes RF, Franca JG. Visual response properties of pretectal units in the nucleus of the optic tract of the opossum. *Exp Brain Res* 78: 380–386, 1989. doi:10.1007/BF00228910.
  47. Wylie DR, Shaver SW, Frost BJ. The visual response properties of neurons in the nucleus of the basal optic root of the northern saw-whet owl (*Aegolius acadicus*). *Brain Behav Evol* 43: 15–25, 1994. doi:10.1159/000113620.
  48. Wylie DR, Frost BJ. The visual response properties of neurons in the nucleus of the basal optic root of the pigeon: a quantitative analysis. *Exp Brain Res* 82: 327–336, 1990. doi:10.1007/BF00231252.
  49. Wylie DRW, Frost BJ. The pigeon optokinetic system: visual input in extraocular muscle coordinates. *Vis Neurosci* 13: 945–953, 1996. doi:10.1017/S0952523800009172.
  50. Wylie DRW, Crowder NA. Spatiotemporal properties of fast and slow neurons in the pretectal nucleus lentiformis mesencephali in pigeons. *J Neurophysiol* 84: 2529–2540, 2000. doi:10.1152/jn.2000.84.5.2529.
  51. Goller B, Altshuler DL. Hummingbirds control hovering flight by stabilizing visual motion. *Proc Natl Acad Sci USA* 111: 18375–18380, 2014. doi:10.1073/pnas.1415975111.
  52. Gaede AH, Goller B, Lam JPM, Wylie DR, Altshuler DL. Neurons responsive to global visual motion have unique tuning properties in hummingbirds. *Curr Biol* 27: 279–285, 2017. doi:10.1016/j.cub.2016.11.041.
  53. Klauer S, Sengpiel F, Hoffmann KP. Visual response properties and afferents of nucleus of the optic tract in the ferret. *Exp Brain Res* 83: 178–189, 1990. doi:10.1007/BF00232207.
  54. Maekawa K, Takeda T, Kimura M. Responses of the nucleus of the optic tract neurons projecting to the nucleus reticularis tegmenti pontis upon optokinetic stimulation in the rabbit. *Neurosci Res* 2: 1–25, 1984. doi:10.1016/0168-0102(84)90002-6.
  55. Wylie DR. Processing of visual signals related to self-motion in the cerebellum of pigeons. *Front Behav Neurosci* 7: 4, 2013. doi:10.3389/fnbeh.2013.00004.
  56. Gutierrez-Ibanez C, Gaede AH, Dannish MR, Altshuler DL, Wylie DR. The retinal projection to the nucleus lentiformis mesencephali in zebra finch (*Taeniopygia guttata*) and Anna's hummingbird (*Calypte anna*). *J Comp Physiol A Neuroethol Sens Neural Behav Physiol* 204: 369–376, 2018. doi:10.1007/s00359-018-1245-5.
  57. Karten JH, Fite KV, Brecha N. Specific projection of displaced retinal ganglion cells upon the accessory optic system in the pigeon (*Columba livia*). *Proc Natl Acad Sci USA* 74: 1753–1756, 1977. doi:10.1073/pnas.74.4.1753.
  58. Wylie DR, Kolominsky J, Graham DJ, Lisney TJ, Gutierrez-Ibanez C. Retinal projection to the pretectal nucleus lentiformis mesencephali in pigeons (*Columba livia*): Retinal projection to lentiformis mesencephali. *J Comp Neurol* 522: 3928–3942, 2014. doi:10.1002/cne.23649.
  59. Gaede AH, Gutierrez-Ibanez C, Armstrong MS, Altshuler DL, Wylie DR. Pretectal projections to the oculomotor cerebellum in hummingbirds (*Calypte anna*), zebra finches (*Taeniopygia guttata*), and pigeons (*Columba livia*). *J Comp Neurol* 527: 2644–2658, 2019. doi:10.1002/cne.24697.
  60. Pakan JMP, Graham DJ, Wylie DR. Organization of visual mossy fiber projections and zebrin expression in the pigeon vestibulocerebellum. *J Comp Neurol* 518: 175–198, 2010. doi:10.1002/cne.22192.
  61. Pakan JMP, Wylie DRW. Two optic flow pathways from the pretectal nucleus lentiformis mesencephali to the cerebellum in pigeons (*Columba livia*). *J Comp Neurol* 499: 732–744, 2006. doi:10.1002/cne.21108.
  62. Wylie DRW. Projections from the nucleus of the basal optic root and nucleus lentiformis mesencephali to the inferior olive in pigeons (*Columba livia*). *J Comp Neurol* 429: 502–513, 2001. doi:10.1002/1096-9861(20010115)429:3<502::AID-CNE10>3.0.CO;2-E.
  63. Crowder NA, Lehmann H, Parent MB, Wylie DRW. The accessory optic system contributes to the spatio-temporal tuning of motion-sensitive pretectal neurons. *J Neurophysiol* 90: 1140–1151, 2003. doi:10.1152/jn.00653.2002.
  64. Crowder NA, Dawson MRW, Wylie DRW. Temporal frequency and velocity-like tuning in the pigeon accessory optic system. *J Neurophysiol* 90: 1829–1841, 2003. doi:10.1152/jn.00654.2002.
  65. Crowder NA, Dickson CT, Wylie DRW. Telencephalic input to the pretectum of pigeons: an electrophysiological and pharmacological inactivation study. *J Neurophysiol* 91: 274–285, 2004. doi:10.1152/jn.00763.2003.
  66. Crowder NA, Wylie DR. Fast and slow neurons in the nucleus of the basal optic root in pigeons. *Neurosci Lett* 304: 133–136, 2001. doi:10.1016/S0304-3940(01)01734-7.
  67. Priebe NJ, Cassanello CR, Lisberger SG. The neural representation of speed in macaque area MT/V5. *J Neurosci* 23: 5650–5661, 2003. doi:10.1523/JNEUROSCI.23-13-05650.2003.
  68. Baliga VB. gaussplotR: Fit, Predict and Plot 2D Gaussians (Online). <https://CRAN.R-project.org/package=gaussplotR> [2021 Sep 16].
  69. Hadfield JD. MCMC methods for multi-response generalized linear mixed models: the MCMCglmm R package. *J Stat Softw* 33: 1–22, 2010. doi:10.18637/jss.v033.i02.
  70. Ibbotson MR. Visual neuroscience: unique neural system for flight stabilization in hummingbirds. *Curr Biol* 27: R58–R61, 2017. doi:10.1016/j.cub.2016.11.052.
  71. Collewijn H. Optokinetic eye movements in the rabbit: input-output relations. *Vision Res* 9: 117–132, 1969. doi:10.1016/0042-6989(69)90035-2.
  72. Gianni H. Stabilizing gaze reflexes in the pigeon (*Columba livia*). *Exp Brain Res* 69: 567–582, 1988. doi:10.1007/BF00247310.
  73. Ibbotson MR, Price NSC. Spatiotemporal tuning of directional neurons in mammalian and avian pretectum: a comparison of physiological properties. *J Neurophysiol* 86: 2621–2624, 2001. doi:10.1152/jn.2001.86.5.2621.
  74. Simpson JI, Graf W. Eye-muscle geometry and compensatory eye movements in lateral-eyed and frontal-eyed animals. *Ann N Y Acad Sci* 374: 20–30, 1981. doi:10.1111/j.1749-6632.1981.tb30856.x.
  75. Suzuki Y, Straumann D, Simpson JI, Hepp K, Hess BJM, Henn V. Three-dimensional extraocular motoneuron innervation in the rhesus monkey. *Exp Brain Res* 126: 187–199, 1999. doi:10.1007/s002210050728.
  76. Van der Steen J, Simpson JI, Tan J. Functional and anatomic organization of three-dimensional eye movements in rabbit cerebellar flocculus. *J Neurophysiol* 72: 31–46, 1994. doi:10.1152/jn.1994.72.1.31.
  77. Oyster CW. The analysis of image motion by the rabbit retina. *J Physiol* 199: 613–635, 1968. doi:10.1113/jphysiol.1968.sp008671.

78. **Frost BJ, Wylie DRW.** A common frame of reference for the analysis of optic flow and vestibular information. *Int Rev Neurobiol* 44: 121–140, 2000. doi:10.1016/s0074-7742(08)60740-0.
79. **Wylie DR, Frost BJ.** Responses of pigeon vestibulocerebellar neurons to optokinetic stimulation. II. The 3-dimensional reference frame of rotation neurons in the flocculus. *J Neurophysiol* 70: 2647–2659, 1993. doi:10.1152/jn.1993.70.6.2647.
80. **Wylie DRW, Frost BJ.** Responses of neurons in the nucleus of the basal optic root to translational and rotational flowfields. *J Neurophysiol* 81: 267–276, 1999. doi:10.1152/jn.1999.81.1.267.
81. **Voogd J, Wylie DRW.** Functional and anatomical organization of floccular zones: a preserved feature in vertebrates. *J Comp Neurol* 470: 107–112, 2004. doi:10.1002/cne.11022.
82. **Weber JT.** Pretectal complex and accessory optic system of primates (part 1 of 2). *Brain Behav Evol* 26: 117–128, 1985. doi:10.1159/000118771.
83. **Iwaniuk AN, Wylie DR.** Sensory systems in birds: what we have learned from studying sensory specialists. *J Comp Neurol* 528: 2902–2918, 2020. doi:10.1002/cne.24896.
84. **Wu S, Amari S, Nakahara H.** Population coding and decoding in a neural field: a computational study. *Neural Comput* 14: 999–1026, 2002. doi:10.1162/089976602753633367.
85. **Olshausen BA, Field DJ.** Emergence of simple-cell receptive field properties by learning a sparse code for natural images. *Nature* 381: 607–609, 1996. doi:10.1038/381607a0.
86. **Gutiérrez-Ibáñez C, Iwaniuk AN, Wylie DR.** Relative size of auditory pathways in symmetrically and asymmetrically eared owls. *Brain Behav Evol* 78: 286–301, 2011. doi:10.1159/000330359.
87. **Knudsen EI, Konishi M.** Space and frequency are represented separately in auditory midbrain of the owl. *J Neurophysiol* 41: 870–884, 1978. doi:10.1152/jn.1978.41.4.870.
88. **Konishi M.** Coding of auditory space. *Annu Rev Neurosci* 26: 31–55, 2003. doi:10.1146/annurev.neuro.26.041002.131123.
89. **Lesica NA, Lingner A, Grothe B.** Population coding of interaural time differences in gerbils and barn owls. *J Neurosci* 30: 11696–11702, 2010. doi:10.1523/JNEUROSCI.0846-10.2010.
90. **Spanne A, Jörntell H.** Questioning the role of sparse coding in the brain. *Trends Neurosci* 38: 417–427, 2015. doi:10.1016/j.tins.2015.05.005.
91. **Niven JE, Laughlin SB.** Energy limitation as a selective pressure on the evolution of sensory systems. *J Exp Biol* 211: 1792–1804, 2008. doi:10.1242/jeb.017574.
92. **Karten HJ, Shimizu T.** The origins of neocortex: connections and lamination as distinct events in evolution. *J Cogn Neurosci* 1: 291–301, 1989. doi:10.1162/jocn.1989.1.4.291.
93. **Miceli D, Peyrichoux J, Repérant J, Weidner C.** Anatomical study of the afferent pathways of the rostral telencephalon in the Gallus domesticus chick. *J Hirnforsch* 21: 627–646, 1980.
94. **Miceli D, Repérant J, Villalobos J, Dionne L.** Extratelencephalic projections of the avian visual Wulst. A quantitative autoradiographic study in the pigeon *Columbia livia*. *J Hirnforsch* 28: 45–57, 1987.
95. **Rio JP, Villalobos J, Miceli D, Repérant J.** Efferent projections of the visual Wulst upon the nucleus of the basal optic root in the pigeon. *Brain Res* 271: 145–151, 1983. doi:10.1016/0006-8993(83)91375-6.
96. **Wylie DRW, Ogilvie CJ, Crowder NA, Barkley RR, Winship IR.** Telencephalic projections to the nucleus of the basal optic root and pretectal nucleus lentiformis mesencephali in pigeons. *Vis Neurosci* 22: 237–247, 2005. doi:10.1017/S0952523805221090.
97. **Berson DM, Graybiel AM.** Some cortical and subcortical fiber projections to the accessory optic nuclei in the cat. *Neuroscience* 5: 2203–2217, 1980. doi:10.1016/0306-4522(80)90137-2.
98. **Grasse KL, Cynader MS.** The accessory optic system in frontal-eyed animals. In: *Vision and Visual Dysfunction. The Neuronal Basis of Visual Function*, edited by Leventhal A. New York: Macmillan, 1990, p. 111–139.
99. **Hoffmann K-P, Distler C, Erickson R.** Functional projections from striate cortex and superior temporal sulcus to the nucleus of the optic tract (NOT) and dorsal terminal nucleus of the accessory optic tract (DTN) of macaque monkeys. *J Comp Neurol* 313: 707–724, 1991. doi:10.1002/cne.903130413.
100. **Ilg UJ, Hoffmann K-P.** Motion perception during saccades. *Vision Res* 33: 211–220, 1993. doi:10.1016/0042-6989(93)90159-T.
101. **Marcotte RR, Updyke BV.** Cortical visual areas of the cat project differentially onto the nuclei of the accessory optic system. *Brain Res* 242: 205–217, 1982. doi:10.1016/0006-8993(82)90302-X.
102. **Mustari MJ, Fuchs AF, Kaneko CRS, Robinson FR.** Anatomical connections of the primate pretectal nucleus of the optic tract. *J Comp Neurol* 349: 111–128, 1994. doi:10.1002/cne.903490108.
103. **Schoppmann A.** Projections from areas 17 and 18 of the visual cortex to the nucleus of the optic tract. *Brain Res* 223: 1–17, 1981. doi:10.1016/0006-8993(81)90802-7.
104. **Shintani T, Hoshino K, Meguro R, Kaiya T, Norita M.** A light and electron microscopic analysis of the convergent retinal and visual cortical projections to the nucleus of the optic tract (NOT) in the pigmented rat. *Neurobiology (Bp)* 7: 445–460, 1999.
105. **Lui F, Giolli RA, Blanks RH, Tom EM.** Pattern of striate cortical projections to the pretectal complex in the guinea pig. *J Comp Neurol* 344: 598–609, 1994. doi:10.1002/cne.903440408.
106. **Holländer H, Tietze J, Distel H.** An autoradiographic study of the subcortical projections of the rabbit striate cortex in the adult and during postnatal development. *J Comp Neurol* 184: 783–793, 1979. doi:10.1002/cne.901840410.
107. **Grasse KL, Cynader MS, Douglas RM.** Alterations in response properties in the lateral and dorsal terminal nuclei of the cat accessory optic system following visual cortex lesions. *Exp Brain Res* 55, 1984. doi:10.1007/BF00240499.
108. **Hoffmann KP.** Cortical versus subcortical contributions to the optokinetic reflex in the cat. In: *Functional basis of ocular motility disorders*, edited by Lennerstrand G, Zee DS, Keller EL. Oxford: Pergamon Press, 1982, p. 303–310.
109. **Ilg UJ, Hoffmann K-P.** Responses of neurons of the nucleus of the optic tract and the dorsal terminal nucleus of the accessory optic tract in the awake monkey. *Eur J Neurosci* 8: 92–105, 1996. doi:10.1111/j.1460-9568.1996.tb01170.x.